BIOCHEMISTRY
including biophysical chemistry & molecular biology

Article

pubs.acs.org/biochemistry

Four-Fold Channels Are Involved in Iron Diffusion into the Inner Cavity of Plant Ferritin

Chenyan Lv,[†] Shengli Zhang,[†] Jiachen Zang,[†] Guanghua Zhao,*[,†] and Chuanshan Xu*[,‡]

[†]CAU & ACC Joint-Laboratory of Space Food, College of Food Science and Nutritional Engineering, China Agricultural University, Beijing Key Laboratory of Functional Food from Plant Resources, Beijing 100083, China

[‡]School of Chinese Medicine (SCM), Chinese University of Hong Kong, Hong Kong, China

Supporting Information

ABSTRACT: From an evolutionary point of view, plant and animal ferritins arose from a common ancestor, but plant ferritin exhibits different features as compared with the animal analogue. One major difference is that the 4-fold channels naturally occurring in plant ferritin are hydrophilic, whereas the 4-fold channels in animal ferritin are hydrophobic. Prior to this study, however, the function of the 4-fold channels in oxidative deposition of iron in phytoferritin remained unknown. To elucidate the role of the 4-fold channels in iron oxidative deposition in ferritin, three mutants of recombinant soybean seed H-2 ferritin (rH-2) were prepared by site-directed mutagenesis, which contained H193A/H197A, a 4-fold channel mutant, E165I/E167A/E171A, a 3-fold channel mutant, and E165I/E167A/E171A/H193A/H197A, where both 3- and 4-channels were mutated. Stopped-flow, electrode oximetry, and transmission electron microscopy (TEM) results showed that H193A/H197A and E165I/E167A/E171A exhibited a similar catalyzing activity of iron oxidation with each other, but a pronounced low activity compared to rH-2, demonstrating that both the 4-fold and 3-fold hydrophilic channels are necessary for iron diffusion in ferritin, followed by oxidation. Indeed, among all tested ferritin, the catalyzing activity of E165I/E167A/E171A/H193A/H197A was weakest because its 3- and 4- fold channels were blocked. These findings advance our understanding of the function of 4-fold channels of plant ferritin and the relationship of the structure and function of ferritin.

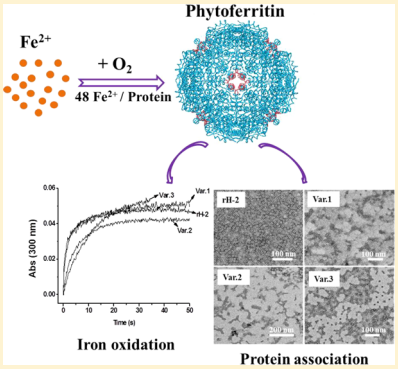

Iron is an essential nutrient involved in cellular functions related to binding and transport of oxygen, redox reactions, detoxification, and nucleotide synthesis.[1,2] However, free iron is toxic because it facilitates the generation of highly reactive oxygen species (ROS) via their on-catalyzed reactions:

$$Fe^{2+} + O_2 \rightarrow O_2^{\bullet -} + Fe^{3+} \quad (1)$$

$$2O_2^{\bullet -} + 2H^+ \rightarrow H_2O_2 + O_2 \quad (2)$$

$$Fe^{2+} + H_2O_2 \rightarrow Fe^{3+} + HO^- + HO^{\bullet} \quad (3)$$

All these ROS can damage cellular constituents. Therefore, iron homeostasis needs to be controlled strictly to avoid iron deficiency and toxicity. Ferritins are ubiquitous iron mineralization proteins and play important roles in iron storage and detoxification within the cell.[3,4] This specific protein is composed of 24 subunits that are arranged in an octahedral (432) symmetry to form a hollow protein shell (outside diameter is 12−13 nm, and inside diameter is 7−8 nm). Although each ferritin molecule has 6 of 4-fold axes, 8 of 3-fold axes, and 12 of 2-fold axes, there are two clearly discernible channels leading from the outside to the inside of the protein shell along the 4-fold and 3-fold axes of symmetry. The three-dimensional structure is very well conserved throughout the animal, plant, and microbial kingdoms. The protein shell can house up to 4500 iron atoms in hydrous ferric oxide forms within its cavity.[5]

In vertebrates, most of the ferritins usually consist of two types of subunits, H (heavy) and L (light), with apparent molecular weights of 21 and 19.5 kDa, respectively. The two subunits have about 55% identity in their amino acid sequence. The H-subunit contains a dinuclear ferroxidase center necessary for iron uptake and for oxidation of ferrous iron. In contrast, the L-subunit lacks a ferroxidase center but contains a putative nucleation site important for slower iron oxidation and mineralization.[6] Structural analyses indicate that each subunit is composed of a four-α-helix bundle containing two antiparallel helix pairs (A, B and C, D) and a fifth short helix (E helix). The E helix lies at one end of the bundle at about 60° to its axis.[1]

Compared with animal ferritin, plant ferritin exhibits different structural features although they arose from a common ancestor. First, only the H subunit has been identified in plant ferritin thus far, and it shares about 40% sequence identity with the animal H subunit.[7,8] The amino acids (Glu27, Tyr34, Glu62, His65, Glu107, and Gln141) involved in the definition of the ferroxidase center are strictly conserved in all reported

Received: January 15, 2014
Revised: February 24, 2014
Published: March 28, 2014

plant ferritins.[11] Second, the subunits of phytoferritins are synthesized as a precursor (32 kDa) with a unique two-domain N-terminal sequence, a transit peptide (TP), and an extension peptide (EP). The TP is presumed to facilitate the transport of the ferritin precursor to plastids.[9] This specific peptide is then cleaved from the subunit precursor, resulting in the formation of the mature subunit, which assembles into a 24-mer apoferritin within a plastid.[10] Thus, in mature plant ferritin, there are 24 EP domains located on its outer surface.[11] Recent studies from our group have revealed that the EP plays an important role in iron transport into and out of phytoferritin.[12−14] Third, each 4-fold channel in plant ferritin is lined with eight histidines[11] and thus is more hydrophilic when compared to those in animal ferritin, which are mainly rich in leucines and more hydrophobic.[1−3,11] However, to date, the function of the hydrophilic 4-fold channels in plant ferritin remains unknown.

Ferritin plays a crucial role in maintaining the iron balance of organisms. Iron uptake by animal ferritin corresponds to iron storage, which has been extensively studied recently.[1−4,15] The migration of Fe^{2+} through the protein shell to the ferroxidase center is believed to be an early event occurring prior to its oxidation in ferritin.[16] An increasing number of evidence supports the belief that the 3-fold hydrophilic channels of animal ferritin are involved in the process.[16−19] Thus, the hydrophilic microenvironment of 3-fold channels seems to provide convenience for iron diffusion into ferroxidase centers. However, the 4-fold channels of plant ferritin are also hydrophilic, a property just like their 3-fold analogues, and what is their function during the iron oxidative deposition process? That is focus of this work. In the present study, we have looked for alternative pathways for iron diffusion into the protein shell during iron oxidative deposition process by using rH-2 (H-2 subunit of soybean seed ferritin) which is more stable than rH-1 (H-1 subunit of soybean seed ferritin). We demonstrated that similar to the 3-fold channels, the 4-fold channels of plant ferritin are also the main pathways for iron diffusion into the protein cavity. This finding represents an alternate pathway for iron deposition in plant ferritin.

MATERIALS AND METHODS

Preparation and Purification of rH-2 and Its Variants. cDNA encoding the full-length amino acid sequence of rH-2 (the H-2 subunit of soybeen seed ferritin) was cloned into the pMD18-T vector (TaKaRa, Dalian, China) and verified by DNA sequencing.[8] DNA sequences encoding the mature region of rH-2 were amplified by polymerase chain reaction using the primers P1 (5′-ATACATATGG CTTCAAATGCACCCGCA-3′) and P2 (5′-GCCGGATCCTTATACATGATGTTC-ATCGTG-3′), which contained *NdeI* and *Bam*HI restriction sites, respectively. The resulting fragments were ligated to the *NdeI* and *Bam*HI sites on the expression vector pET 21d (Novagen) to generate pET SferH-2. Three specific mutations were designed for substitutions of Glu165, Glu167, and Glu171 located at the 3-fold channels of rH-2 with Ile, Ala, and Ala, respectively. The other two mutations were designed for substitutions of His193 and His197 located at the 4-fold channels of rH-2 with Ala. Mutagenesis of the rH-2 cDNA was performed with the fast mutagenesis system kit (TransGen Biotech). PCR amplification was carried out using the pET-21d plasmid with the rH-2 gene as a template, E165I: P1 5′-TGGCAGACTTCATTATCAGCGAGTT-3′ and P2 5′-GATGCTCTCAATGAAGTCTGCCAAT-3′, E167A: P1 ACTTCATTATCAGCGCGTTCTTGTA and P2 5′-GCGCT-GATAATGAAGTCTGCCAATT-3′, E171A: P1 5′-GCGCG-TTCTTGTATGCGCAGGTTAA-3′ and P2 5′-GCATA-CAAGAACGCGCTGATAATGA-3′, H193A: P1 5′-AGGGT-GCTGGTGTGTGGCACTTTGA-3′ and P2 5′-GCACCCTTTCCAACTAATCTCAGT-3′, H197A: 5′-TGTATGGGCCTTCGATCAAAAGCTTC-3′ and P2 5′-GCCCACACACCAGCACCCTTTCCAA-3′ as primers. PCR amplification was as follows: denaturation at 94 °C for 5 min, followed by 30 cycles of 94 °C for 30 s, 55 °C for 30 s, and 72 °C for 2 min, and a final extension cycle of 72 °C for 10 min. After the PCR reaction, the parental DNA template was digested with DMT enzyme. The PCR amplified plasmid was separated on agarose gel, extracted, and inserted into *Escherichia coli* competent cells. Ampicillin-resistant colonies were selected from which the plasmids were extracted. The extracted plasmid was sequenced for confirmation of the site-directed mutation.[20]

The expression plasmids pET rH-2 and pET mutants were transformed into the *E. coli* strain BL21 (DE3), respectively. The positive transformants of each construct were grown at 37 °C on LB medium supplemented with 50 mg/L ampicillin, and protein expression was induced with 1 mM isopropyl-β-D-1-thiogalactopyranoside when the cell density reached an absorbance of 0.6. The cells were harvested by centrifugation, followed by disruption by sonication. Three kinds of proteins were obtained, variant #1 (H193A/H197A), variant #2 (E165I/E167A/E171A), and variant #3 (H193A/H197A/E165I/E167A/E171A). rH-2 and its mutants were purified according to the purification method for soybean seed ferritin.[21] The concentrations of all types of ferritin were determined according to the Lowry method with BSA as a standard sample.

Polyacrylamide Gel Electrophoresis. The molecular weight of the rH-2 and its mutants were estimated by polyacrylamide gel electrophoresis using a 4−20% polyacrylamide gradient gel run at 25 V for 14 h at 4 °C employing Tris-HCl (25 mM, pH 8.3) as a running buffer. Gels were stained with Coomassie Brilliant Blue R250. Gel electrophoresis under denaturing conditions was carried out with 15% polyacrylamide-SDS gel as reported by Laemmli.[22] Protein samples (~20 μg) were suspended in 50 μL of water. To the solution was added 100 μL of sample buffer containing 25% glycerol, 12.5% 0.5 M Tris-HCl, pH 6.8, 2% SDS, 1% bromophenol blue, and 5% β-mercaptoethanol. For native PAGE, the SDS was replaced with water. All quoted concentrations were final concentrations. After the solution was boiled for 10 min, the supernatant was isolated by centrifugation at 10000*g* for 10 min.

Circular Dichroism (CD) and Fluorescence Spectroscopy. CD spectra were recorded on a PiStar-180 spectrometer (Applied Photophysics) at room temperature (25 ± 1 °C) under a constant flow of nitrogen gas. A total of 0.5 mL of rH-2 (0.25 μM) and its mutants in 10 mM PBS (pH 7.2) was warmed to room temperature prior to analysis. Each sample was scanned in the range of 180−260 nm. A CD spectrum was obtained as the average of four scans with the 50 mM PBS background subtracted.

Fluorescence measurements were run on a Cary Eclipse spectrofluorimeter (Varian). Excitation−emission spectra were measured at 25 °C and processed to obtain the emission spectra (λ_{em}: 310−550 nm) at the maximum excitation wavelength (295 nm). Protein concentrations are 0.25 μM. All measurements were performed in triplicate.

Fe^{2+} Oxidative Deposition in Ferritin. The fast kinetic experiments were undertaken with the pneumatic drive Hi-

dx.doi.org/10.1021/bi500066m | *Biochemistry* 2014, 53, 2232−2241

Tech SFA-20M stopped flow accessory on a Varian Cary 50 spectrophotometer (Varian, USA). The weakly acidic $FeSO_4$ solution was freshly prepared before use with pH 2.0 ddH_2O (the pH value of ddH_2O was adjusted to 2.0 with 1.0 M HCl). Equal 140 μL volumes of a weakly acidic $FeSO_4$ solution (48, 96, 200, and 500 μM) and buffered apoferritin solution (1.0 μM) were mixed at 25 °C in the thermostated sample compartment containing a 280 μL quartz stopped flow cuvette with 1 cm optical path length. μ-oxo di-Fe^{3+} species formed during Fe^{2+} oxidation were monitored by 300 nm. Data were acquired every 12.5 ms (the shortest acquisition time possible with the Cary 50). The spectrophotometer was operated in single beam mode and zeroed prior to each kinetic run with a cuvette containing apoferritin in buffer. The kinetic data was curve fitted with Origin 8.0 software (Micro Cal Inc.). The initial rate (v_0) of iron oxidation measured as μ-oxo complex formation was obtained as previously described.[12,13] All experiments and measurements were performed in triplicate.

Kinetics of Oxygen Consumption. The kinetics of oxygen consumption was monitored in a specially designed 0.48 mL reaction cell fitted with an oxygen microelectrode (MI730). The protein concentration is 1.0 μM. The electrode oximetry apparatus and standardization reactions were carried out as previously described.[23] All experiments and measurements were performed in triplicate.

Characterization of Ferritin by Transmission Electron Microscopy (TEM). TEM data were collected at different iron loadings (48, 200, and 500 Fe^{2+}/shell) by a Hitachi S-5500 transmission electron microscope operating at 30 kV. TEM experiments were performed in which Fe^{2+} was rapidly mixed with apo phytoferritin (rH-2, H193A/H197A, E165I/E167A/E171A, and E165I/E167A/E171A/H193A/H197A) under aerobic conditions and then transferred to carbon-coated copper grids. The concentration of all samples was 0.05 μM. The samples were negative stained with uranyl acetate.[24] All experiments were performed in triplicate.

Kinetics of Iron Release. Iron release from holoferritin was investigated by using the assay procedure previously described.[25] Reconstituted holoferritin with 800 iron atoms was prepared by adding 800 Fe^{2+} to apoferritin in one shot, followed by standing overnight as previously described.[15] Briefly, the assay system (1 mL of total volume) contained 0.2 μM holoferritin, 500 μM ferrozine, and 0.15 M NaCl in 50 mM Mops buffer (pH 7.0). Reactions were carried out at 25 °C and were initiated by the addition of ascorbic acid (1 mM). The development of $[Fe(ferrozine)_3]^{2+}$ was measured by recording the increase in absorbance at 562 nm using a Varian Cary 50 spectrophotometer, using $\varepsilon_{562\ nm}$ = 27.9 mM^{-1} cm^{-1}. The kinetic data were further analyzed with Origin 8.0 software (Micro Cal Inc.). The initial rate of iron release (v_0) was obtained from the linear A_1 term of a third-order polynomial fitted to the experimental data as described previously: namely, $Y = A_0 + A_1t + A_2t^2 + A_3t^3$ and $dY/dt = A_1 + 2A_2t + 3A_3t^2$ (at t = 0, $(dY/dt)_0 = v_0$). Here t is the time in seconds, and Y is the concentration of $[Fe(ferrozine)_3]^{2+}$ at time t in seconds. All experiments and measurements were performed in triplicate.

RESULTS

Purification and Characterization of rH-2 and Its Mutants. Nondenaturing polyacrylamide gel electrophoresis (native PAGE) showed that rH-2 and its three mutants, which included a 4-fold channel variant #1 (H193A/H197A), a 3-fold channel variant #2 (E165I/E167A/E171A), and a 3-fold and 4-fold channels variant #3 (H193A/H197A/E165I/E167A/E171A), were purified to homogeneity and had nearly the same apparent molecular weights (MWs) of around 560 kDa at pH 8.3 (Figure 2A) as previously reported.[13] SDS-PAGE

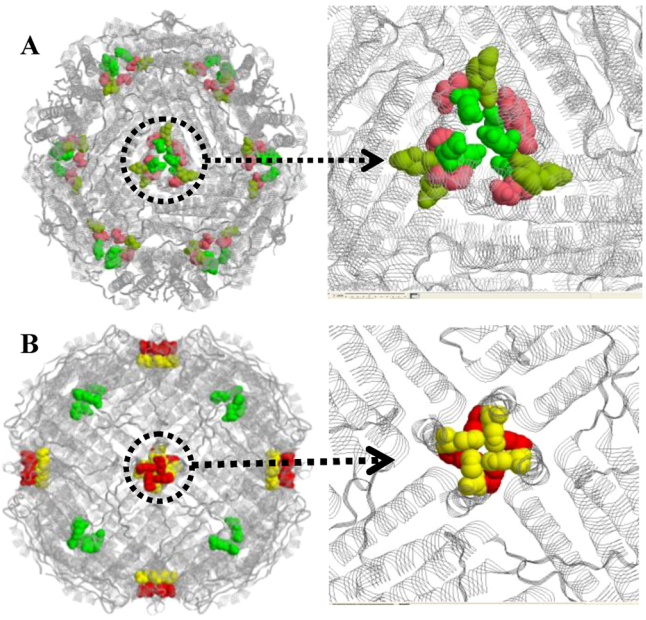

Figure 1. Phytoferritin shell with views down the 3-fold (A) and 4-fold (B) axes of the protein shell. The full protein shell is shown on the left with the rotation symmetry. An expanded view of each type of channel is shown on the right with key residues indicated. (A) The 3-fold channel with Glu163 (green), Glu165 (pink), and Glu169 (yellow green). (B) The 4-fold channel with His195 (yellow) and His199 (red).

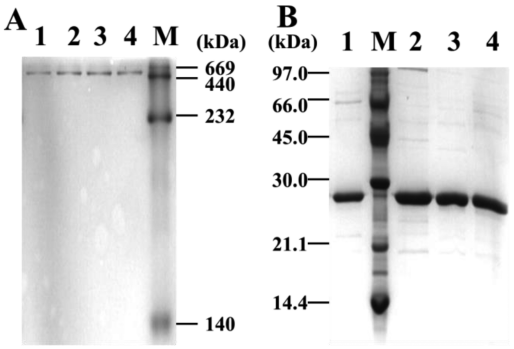

Figure 2. Native PAGE and SDS-PAGE analyses of purified rH-2 and its variants. (A) Native PAGE. (B) SDS-PAGE. Lane 1, rH-2; Lane 2, H193A/H197A; Lane 3, E165I/E167A/E171A; Lane 4, E165I/E167A/E171A/H193A/H197A; Lane M, protein markers and their corresponding molecular masses.

showed that these three mutants were composed of 24 identical subunits, the MW of which is nearly the same as rH-2 (7) (Figure 2B). These results indicate that site-directed mutation has not affected their electrophoretic behavior.

To elucidate the effect of site-directed mutation on protein secondary structure, rH-2 and its mutants were studied with far UV-CD spectroscopy. Changes in far UV-CD correspond to alteration in the overall secondary structure of the protein.[26] The native form of rH-2, H193A/H197A, E165I/E167A/E171A, H193A/H197A/E165I/E167A/E171A all had very similar two negative ellipticities in the far-UV spectrum, at

dx.doi.org/10.1021/bi500066m | Biochemistry 2014, 53, 2232−2241

208 and 222 nm, which was in good agreement with the previous reports for the secondary structure of plant, animal, and bacterial ferritin,[1−4,27] indicating that such mutations hardly affect the secondary structure of ferritin (Figure 3A).

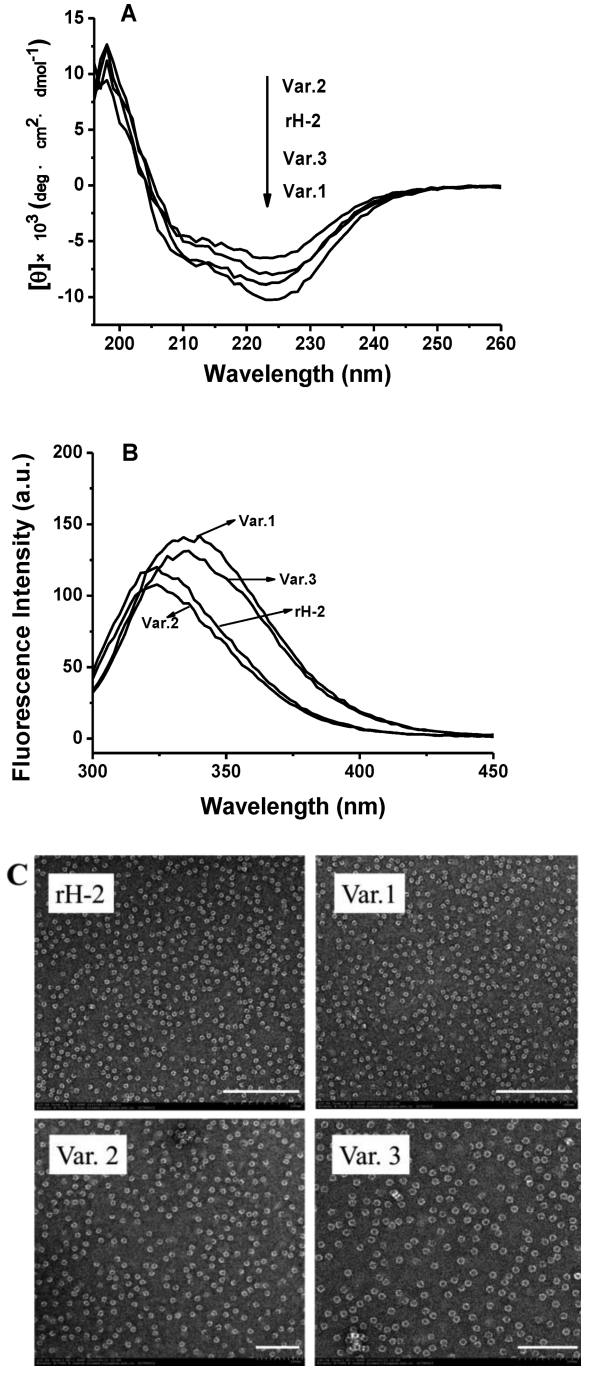

Figure 3. (A) CD spectra of rH-2 and its variants. CD spectrum was obtained as the average of four scans with the 50 mM PBS background subtracted. (B) Fluorescence emission spectra of rH-2 and its variants. The excitation wavelength of rH-2 and its variants was 295 nm. Conditions: [apo rH-2, Var. 1 (H193A/H197A), Var. 2 (E165I/E167A/E171A), Var. 3 (E165I/E167A/E171A/H193A/H197A)] = 0.25 μM in 10 mM PBS (pH 7.2), 25 °C. (C) Transmission electron microscope analysis of rH-2 and its variants [apo rH-2, Var. 1 (H193A/H197A), Var. 2 (E165I/E167A/E171A), Var. 3 (E165I/E167A/E171A/H193A/H197A)] = 0.05 μM. All other measurements were performed in triplicate.

Meanwhile, fluorescence spectroscopy has been shown to be a very useful technique for studying structure and dynamics in protein. The intrinsic fluorescence emission from tryptophan residue in proteins is sensitive to the microenvironment surrounding the fluorophore residue.[28] As shown in Figure 3B, rH-2 exhibited a strong fluorescence peak at 324 nm when excited at 280 nm, indicating that most of the observed fluorescence is contributed by the sole tryptophan residue Trp196 located on the 4-fold channels, in agreement with a previous report.[8] In contrast, there is a significant red shift for both H193AH197A and E165I/E167A/E171A/H193A/H197A, and their maximum emission wavelength is at around 336 nm, because His197, a residue most close to Trp196, was replaced by hydrophobic amino acids (Ala197) in these two variants, and such a mutation resulted in a certain change in the localized tertiary structure around Trp196. As expected, the maximum emission wavelength of the E165I/E167A/E171A, a 3-fold channel variant, is nearly the same as that of rH-2, most likely because mutations in the 3-fold channels are far away from Trp196.

To further probe whether site-directed mutations have affected the shell-like structure of ferritin, all proteins (0.05 μM) (rH-2 and its three variants) were negative stained with uranyl acetate and observed by a transmission electron microscope (TEM), respectively. TEM images revealed that all four molecules had identical shell-like structures with an outside diameter of 12 nm (Figure 3C), demonstrating that sited-directed mutations for all three variants have not destroyed their protein shell-like structure although they have a certain effect on the microenvironment around Trp196 with H193A/H197A and E165I/E167A/E171A/H193A/H197A.

Kinetics of Iron Oxidation in rH-2 and Its Mutants. UV absorption in the 300−330 nm spectral regions has been traditionally used to monitor the formation of Fe^{3+} species during oxidative deposition of iron in the ferritins.[29−31] Spectrophotometric kinetic measurements of iron deposition in rH-2 and its mutants by stopped-flow were conducted to compare their catalytic activity at four different iron loadings (48, 96, 200, and 500 Fe^{2+}/protein) (Figure 4). As shown in Figure 4, the stopped-flow UV−visible kinetic traces are very smooth, suggesting that no insoluble protein aggregates form during iron oxidative deposition in protein. In addition, all curves are hyperbolic, consistent with protein catalysis of iron oxidation.[32]

At low iron loading (48 Fe^{2+}/shell), the initial rate of iron oxidation catalyzed by rH-2 is 0.176 ± 0.006 μM iron/subunit/s are larger than those of both H193A/H197A, a 4-fold channel mutant (0.148 ± 0.009 μM iron/subunit/s) and E165I/E167A/E171A, a 3-fold channel mutant (0.127 ± 0.003 μM iron/subunit/s) when compared on a subunit basis (2 Fe^{2+}/subunit) under the present conditions (Figure 4A), suggesting that both 3-fold channels and 4-fold channels are important pathways for iron diffusion into the ferroxidase centers. Consistent with this idea, the initial rate of iron oxidation catalyzed by E165I/E167A/E171A/H193A/H197A (0.085 ± 0.003 μM iron/subunit/s) is smaller than those of H193A/H197A and E165I/E167A/E171A. Additionally, the initial rate of iron oxidation catalyzed by H193A/H197A is similar to that of E165I/E167A/E171A, indicating that the relative contributions of 3-fold channels and 4-fold channels to iron oxidation are essentially equal (Figure 3A), in accordance with the previous report in prokaryotes.[33]

dx.doi.org/10.1021/bi500066m | *Biochemistry* 2014, 53, 2232−2241

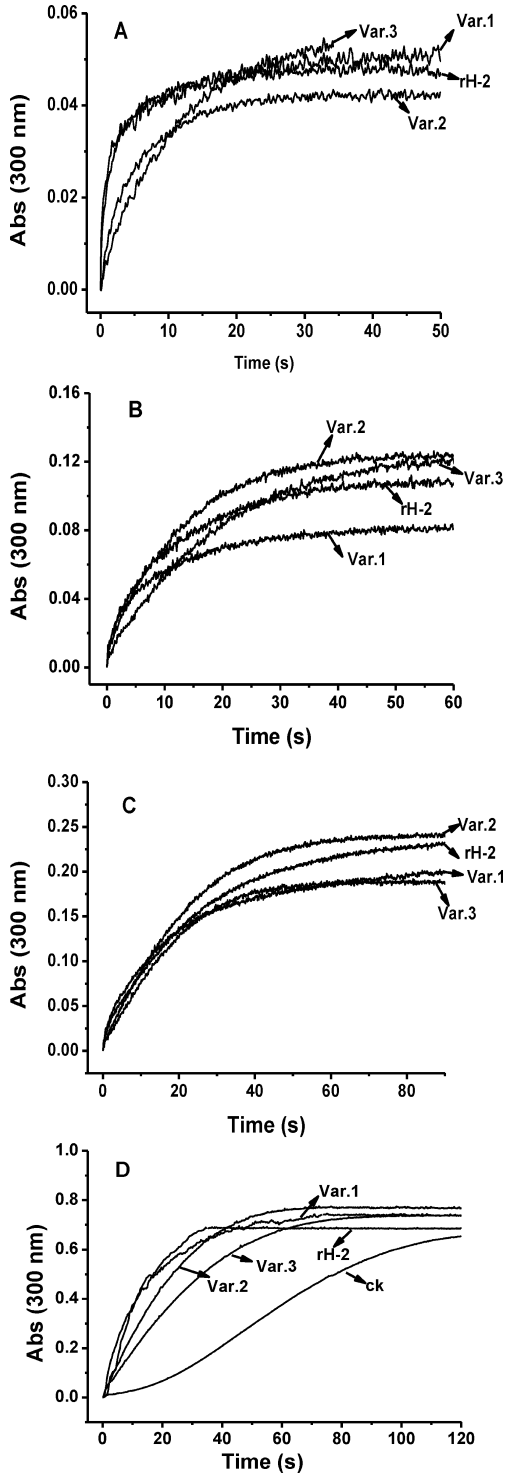

Figure 4. Kinetic curves of Fe^{2+} oxidation by O_2 in the presence of apo rH-2 and its variants (Var.1-H193A/H197A, Var.2-E165I/E167A/E171A, Var.3- E165I/E167A/E171A/H193A/H197A) at different Fe^{2+} concentrations, 48 (A), 96 (B), 200 (C), and 500 Fe^{2+}/shell (D). Conditions [apo rH-2, Var.1-H193A/H197A, Var.2-E165I/E167A/E171A, Var.3-E165I/E167A/E171A/H193A/H197A] = 0.5 μM in 50 mM Mops (pH 7.9), 24–250 μM $FeSO_4$, 25 °C. All the measurements were performed in triplicate.

At intermediate iron loadings (96 Fe^{2+}/shell and 200 Fe^{2+}/shell), biphasic kinetic curves are observed, which are characterized by an initial fast phase followed by a slow phase. The initial rapid rise in absorbance is attributed to fast Fe^{2+} oxidation at the diiron ferroxidase site.[7,12] For rH-2 and its variants, the EP is responsible, at least partially, for iron mineralization in the second phase, consistent with the idea that pea seed ferritin contains at least two kinds of centers for Fe^{2+} oxidation.[12] Meanwhile, the regeneration activity of ferroxidase sites in plant ferritin is low,[34] which is different from that of bullfrog ferritin.[35] At the iron loading of 96 Fe^{2+}/shell, the initial rates of iron oxidation for rH-2 and E165I/E167A/E171A are 0.108 ± 0.002 μM iron/subunit/s and 0.116 ± 0.001 μM iron/subunit/s, respectively, and there is no significant difference between them, which means that the 3-fold channels are not the only pathways for iron diffusion and oxidation at medium iron flux into apoferritin. Consistent with this idea, the initial rates of H193A/H197A (0.086 ± 0.002 μM iron/subunit/s) and E165I/E167A/E171A/H193A/H197A (0.081 ± 0.001 μM iron/subunit/s) are similar and are smaller than that of rH-2 (Figure 4B), indicating that the 4-fold channels play a more important role in iron oxidation than its 3-fold analogues at medium iron loading.

At the iron loading of 200 Fe^{2+}/shell, iron oxidation catalyzed by four ferritins is shown in Figure 4C. There is no significant difference among their initial rates (rH-2, 0.119 ± 0.002 μM iron/subunit/s, H193A/H197A, 0.137 ± 0.002 μM iron/subunit/s, E165I/E167A/E171A, 0.132 ± 0.001 μM iron/subunit/s, and E165I/E167A/E171A/H193A/H197A, 0.110 ± 0.001 μM iron/subunit/s), probably because the oxidative activity of EP domain located at the outer surface of ferritin is very similar at intermediate iron loading (200 Fe^{2+}/shell).[7] The EP domains of these four ferritins are the same, which are mainly responsible for iron oxidation when the diiron ferroxidase centers are saturated with 48 Fe^{3+} and have not been regenerated.[12]

At high iron loading of the protein (500 Fe^{2+}/shell), the conventional kinetic traces obtained at 300 nm are shown in Figure 4D. The curves follow the same general trend reported for additions of 1000 or 2000 Fe^{2+}/protein to ferritin.[36] rH-2 is the most kinetically active of the ferritins followed by H193A/H197A, E165I/E167A/E171A, and E165I/E167A/E171A/H193A/H197A. All of the curves are hyperbolic, consistent with these proteins having fully intact H-chain ferroxidase sites. In contrast, the curve for buffer only shows a sigmoidal behavior with slow initial phase, and such behavior is expected for an autocatalytic mineral surface mechanism.[37] As the iron core grows larger, the EP oxidation pathway becomes less important, because Fe^{2+} oxidation and deposition occur directly on the surface of the iron core.[12] The initial rate of iron oxidation catalyzed by rH-2 (0.971 ± 0.010 μM iron/subunit/s) is ~2-fold larger than that by E165I/E167A/E171A/H193A/H197A (0.366 ± 0.002 μM iron/subunit/s) and ~1-fold larger than that by E165I/E167A/E171A (0.559 ± 0.001 μM iron/subunit/s), again suggesting that 3-fold and 4-fold channels are both important pathways for iron diffusion into protein cage. The same result can come from the comparison of H193A/H197A (0.883 ± 0.008 μM iron/subunit/s) and rH-2. Therefore, the hydrophilic channels of rH-2 including 3-fold and 4-fold ones are main pathways for iron diffusion, oxidation, and deposition.

To further identify the iron diffusion and oxidation mechanism of rH-2 and its variants, the kinetics of oxygen consumption was investigated by oxygen electrode as shown in Figure 5. At low iron loading (48 Fe^{2+}/shell), it can be seen that the Fe(II) oxidation reactions are facilitated by all the ferritins with the reaction initial rates following the order of rH-

dx.doi.org/10.1021/bi500066m | Biochemistry 2014, 53, 2232–2241

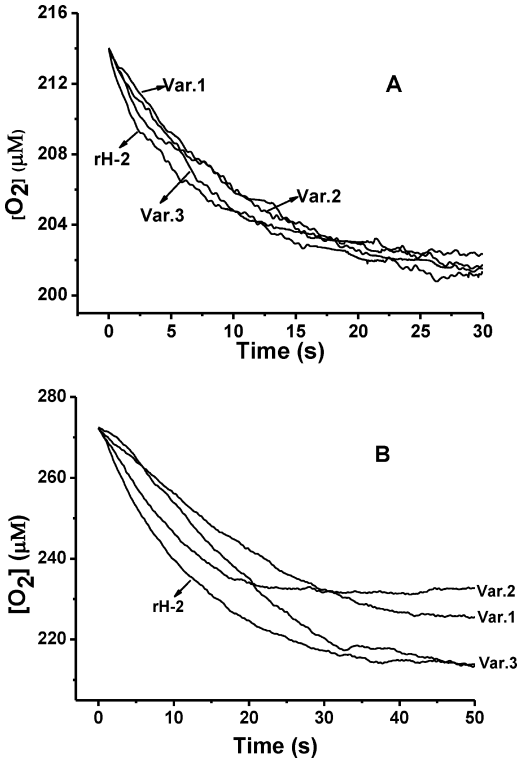

Figure 5. Oxygen consumption versus time for Fe(II) oxidation in the presence of rH-2, Var.1-H193A/H197A, Var.2-E165I/E167A/E171A, and Var.3- E165I/E167A/E171A/H193A/H197A upon different iron loadings. (A) 48 Fe^{2+}/protein shell; (B) 200 Fe^{2+}/protein shell. Conditions: [rH-2 or its variants] = 1.0 μM in 50 mM Mops and 50 mM NaCl (pH7.9); [Fe^{2+}] = 48 μM or 200 μM, [O_2] = 0.28 mM, at 20 °C. All the measurements were performed in triplicate.

2 (1.830 ± 0.030 μM O_2/s) > E165I/E167A/E171A/H193A/H197A (1.489 ± 0.042 μM O_2/s) > E165I/E167A/E171A (1.453 ± 0.020 μM O_2/s) > H193A/H197A (1.027 ± 0.021 μM O_2/s) (Table 2). These findings likewise indicated that both the 3-fold and 4-fold channels are important for iron entry into protein shell followed by oxidation catalyzed by ferritin, which is in a good agreement with the stopped-flow results.

The oxidation of approximately 2 Fe(II) per O_2 for 48 Fe(II)/rH-2 added implies that hydrogen peroxide is a product in this reaction, in accordance with previous findings with HuHF and other ferritins.[23,29] The same result was observed with E165I/E167A/E171A. In contrast, the Fe(II)/O_2 stoichiometry of E165I/E167A/E171A/H193A/H197A is ~1.4/1; this is mainly because Fenton reaction occurs to some extent after almost all channels of iron entry into ferritin were blocked.

Subsequently, the oxygen consumptions of rH-2 and its variants at medium iron loading were investigated (Figure 5B). Upon adding ~200 Fe^{2+} per protein shell to apoferritin, the iron oxidation was not only catalyzed by the ferroxidase centers but also by the EP domains at the outer surface of phytoferritin. The initial rate of rH-2 is 4.560 ± 0.016 μM O_2/s, which is ~2-fold larger than H193A/H197A (1.626 ± 0.013 μM O_2/s) and E165I/E167A/E171A/H193A/H197A (1.816 ± 0.024 μM O_2/s), again suggesting that the 4-fold channels are involved in ferrous ion diffusion, followed by its oxidation.[16] These results are consistent with the above stopped-flow results. Therefore, the hydrophilic 4-fold channels of phytoferritin are the key pathways for iron diffusion and important for iron oxidation. As for E165I/E167A/E171A, the oxygen consumption initial rate is 3.425 ± 0.013 μM O_2/s, smaller than that of rH-2, indicating the hydrophilic 3-fold channels are also the pathways for iron diffusion, as previous studies on animal ferritin reported.[16]

Ferritin Association Property in rH-2 and Its Mutants. At low iron flux into the protein (≤48 Fe^{2+}/protein shell), plant ferritin catalyzes iron oxidation via the diiron ferroxidase center through a ferroxidase mechanism as proposed previously. In contrast, at high iron flux into protein (>48 Fe^{2+}/protein shell), this mechanism is gradually replaced by another mechanism by which the iron oxidation is processed by the EP located on the outer surface of plant ferritin. Our previous studies demonstrated that Fe^{3+}-involved protein association property provides important information on the catalyzing activity of the EP domains, which serves as the second ferroxidase center at high iron loading (>48 Fe^{2+}/protein shell).[12] Therefore, the protein association property was studied with rH-2 and these three mutants by TEM in this work.

At low iron loading (48 Fe^{2+}/shell), rH-2 shells were dispersed uniformly, and the outer diameter is 12 nm (Figure 6A), in accordance with the previous results.[38] In contrast, protein association occurred with variants of rH-2 (H193A/H197A, E165I/E167A/E171A, and E165I/E167A/E171A/H193A/H197A) to different extents. According to the previous study, at a low flux of Fe^{2+} into ferritin (<2 Fe^{2+}/chain), Fe^{2+} oxidation by O_2 is processed completely by the ferroxidase sites with an Fe^{2+}/O_2 stoichiometry of 2:1, and the EP domains are not involved in this process.[12] However, upon replacing the hydrophilic amino acids with hydrophobic ones (H193A/H197A, E165I/E167A/E171A, and E165I/E167A/E171A/H193A/H197A), iron diffusion is greatly compromised, and thus some ferrous ions may bind to the EP domain at the surface of ferritin, followed by a slow oxidation and turnover process. Consequently, ferric ions as oxidative products of ferrous ions caused ferritin association as shown in Figure 6A, demonstrating that like 3-fold channels, the 4-fold channels are necessary for iron diffusion into the ferroxidase center of plant

Table 1. Initial Rates of Fe^{2+} Oxidation by O_2 in the Presence of apo rH-2 and Its Variants[a] at Different Fe^{2+} Concentrations Obtained from Figure 4[b]

	initial rate (μM iron/subunit/s)			
Fe^{2+}/shell	rH-2	H193A/H197A	E165I/E167A/E171A	H193A/H197A/E165I/E167A/E171A
48	0.176 ± 0.006	0.148 ± 0.009	0.127 ± 0.003	0.085 ± 0.003
96	0.108 ± 0.002	0.086 ± 0.002	0.116 ± 0.001	0.081 ± 0.001
200	0.119 ± 0.002	0.137 ± 0.002	0.132 ± 0.001	0.110 ± 0.001
500	0.971 ± 0.010	0.883 ± 0.008	0.559 ± 0.001	0.366 ± 0.002

[a]Var. 1, H193A/H197A; Var. 2, E165I/E167A/E171A; Var. 3, E165I/E167A/E171A/H193A/H197A. [b]Conditions [apo rH-2 or Var. 1 or Var. 2 or Var. 3] = 0.5 μM in 50 mM Mops (pH 7.9), 24–250 μM $FeSO_4$, 25 °C.

dx.doi.org/10.1021/bi500066m | Biochemistry 2014, 53, 2232–2241

Table 2. Initial Rates of Oxygen Consumption in the Presence of rH-2, Var. 1 (H193A/H197A), Var. 2 (E165I/E167A/E171A), and Var. 3 (E165I/E167A/E171A/H193A/H197A) upon Different Iron Loadings[a]

	initial rate (μM O_2/s)			
Fe^{2+}/shell	rH-2	H193A/H197A	E165I/E167A/E171A	H193A/H197A/E165I/E167A/E171A
48	1.830 ± 0.030	1.027 ± 0.021	1.453 ± 0.020	1.489 ± 0.042
200	4.560 ± 0.016	1.626 ± 0.013	3.425 ± 0.013	1.816 ± 0.024

[a]Conditions: [rH-2 or its variants] = 1.0 μM in 50 mM Mops and 50 mM NaCl (pH7.9), [Fe^{2+}] = 48 μM or 200 μM, [O_2] = 0.28 mM, at 20 °C.

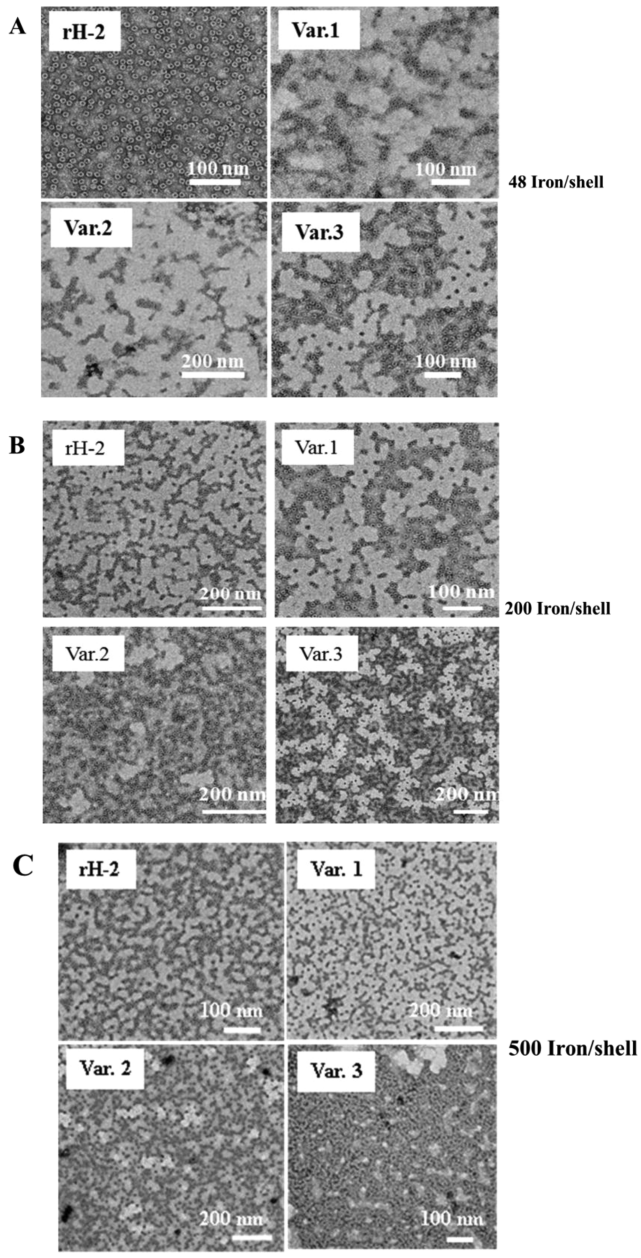

Figure 6. Transmission electron micrographs of apo rH-2, Var.1-H193A/H197A, Var.2-E165I/E167A/E171A, and Var.3-E165I/E167A/E171A/H193A/H197A rapidly loaded with 48 (A), 200 (B), and 500 Fe^{2+}/shell (C), respectively. All samples were negative stained with uranyl acetate. The protein concentration is 0.05 μM in 50 mM Mops, pH 7.9. All the measurements were performed in triplicate.

ferritin, which is in good agreement with the above stopped-flow and electrode oximetry results (Figures 3A and 4A).

In another series of experiments, 200 Fe^{2+}/shell were added to apo rH-2 and its variants. In contrast, all of the ferritins aggregated obviously, the magnitude of the increase being a strong function of the ratio beyond 48 Fe^{2+}/shell (Figure 6B). And there is no significant difference among rH-2 and its variants. This is because the 24 dinuclear ferroxidase centers of rH-2 have a maximal binding capacity of 48 Fe^{3+} and are located in the interior of the protein.[34,39] These results suggest that protein−protein association is facilitated by binding of the additional iron on the exterior surface of protein shell (EP domain). Ferroxidase centers interior and EP domains outside both play crucial roles in this process (200 Fe^{2+}/shell). To further investigate the iron oxidation and deposition, we monitored the association property of ferritin at the iron loading of 500 Fe^{2+}/shell. As expected, rH-2 and its variants aggregated to a greater extent (Figure 6C).

To study the association phenomenon in detail, we undertook light scattering experiments by monitoring the fluorescence intensity of rH-2 and its variants which were rapidly mixed with 500 Fe^{2+}/shell.[12] As shown in Figure S1, Supporting Information, the fluorescence intensity reached a plateau within 40 s, and the scattering intensity of E165I/E167A/E171A/H193A/H197A is higher than other proteins, consistent with TEM observations under same conditions. Hence, the iron diffusion channels seem to be more and more important to this process. The hydrophobic channels of rH-2 variants may impede the transfer of Fe^{3+} from EP domain to the protein inner cavity and the diffusion of additional Fe^{2+} to the mineral core surface, and further hindered the disassociation of ferritin. All this results indicated again that the 3-fold and 4-fold channels are both key pathways for iron diffusion.

It has been established that protein−protein association is facilitated by binding of the additional iron on the exterior surface of protein shell,[7,12,13] because the 24 dinuclear ferroxidase centers of plant ferritin have a maximal binding capacity of 48 iron ions and are located in the interior of the protein. The EP domains as the second feroxidase centers are responsible for oxidation of iron binding on the outer surface. Since both the 3-fold and 4-fold channels were blocked, protein association occurred with E165I/E167A/E171A/H193A/H197A to the largest extent upon addition of 500 Fe^{2+}/protein shell to apoferritin, followed by E165I/E167A/E171A, H193A/H197A, and rH-2. If these ferric ions were bound on the EP located at the exterior surface of protein, one would expect that a fast iron release will be observed and follow the same order as the degree of protein association. To confirm this view, the kinetics of iron release from rH-2 and its three mutants loaded with 800 Fe^{2+}/shell was monitored by absorption at 562 nm, respectively. Generally, the amount of iron released from ferritins increased with time (Figure 7). The iron release initial rate of rH-2 is 2.70 nM/s, which is similar to previous reports under same conditions.[40] In contrast, the initial rate of the 3-fold channel mutant E165I/E167A/E171A is 3.00 nM/s, a value larger than that of rH-2. As for the 4-fold channel mutant H193A/H197A and E165I/E167A/E171A/H193A/H197A, their initial rates are 8.02 nM/s and 7.77 nM/s, respectively,

dx.doi.org/10.1021/bi500066m | Biochemistry 2014, 53, 2232−2241

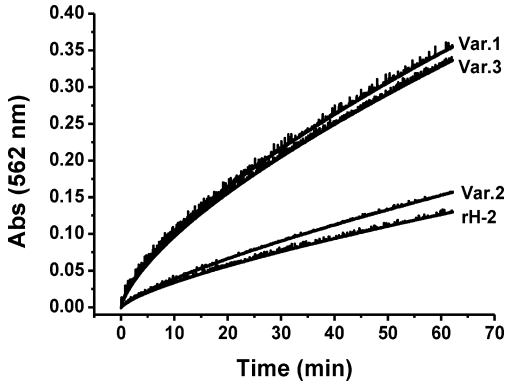

Figure 7. Kinetics of iron release from rH-2, Var. 1 - H193A/H197A, Var. 2 - E165I/E167A/E171A and Var. 3 - E165I/E167A/E171A/H193A/H197A (which have been loaded with 800 Fe^{2+}/shell and kept overnight in advance) induced by ascorbate. Iron release from rH-2 and its variants was followed by measuring the increase in absorbance at 562 nm due to the chelation of Fe^{2+} by ferrozine. Conditions: 0.2 μM rH-2 or its variants, 500 μM ferrozine, and 1 mM ascorbate, in 50 mM Mops and 150 mM NaCl (pH 7.9, 25 °C). All the measurements were performed in triplicate.

and are ~2 fold larger than that rH-2, suggesting that more ferric ions were binding at the outer surface of H193A/H197A and E165I/E167A/E171A/H193A/H197A than rH-2, which is in good accordance with the above TEM results. These results again demonstrated that the 3-fold and 4-fold hydrophilic channels are important for iron diffusion into plant ferritin shell.

DISCUSSION

To date, all known ferritins with three-dimensional structures of 24 structurally equivalent subunits assembled into a cagelike oligomer are highly conserved.[1,41] Ferritins combine the properties of ion-channel proteins and Fe^{2+}/O_2 oxidoreductases. Fe^{2+} passes through the protein nanocage to the active sites, and the Fe^{3+}-O mineral precursors move to the cavity where the bulk mineral grows. Three major metal binding sites have been identified in animal ferritin, which exhibit some common aspects related to the iron storage mechanism: (i) they exist around the 3-fold symmetry channel, (ii) constitute a ferroxidase center in the four-helix bundle, and (iii) constitute a nucleation site facing the inner cavity of ferritin.[42−47] It has been suggested that iron atoms pass through the hydrophilic channels that traverse the ferritin shell around the 3-fold symmetry axes of oligomeric ferritin.[16] This funnel-like channel is surrounded by hydrophilic residues, such as aspartic acid and glutamic acid, which have been demonstrated to serve as ligands for metal ions, such as ferrous, calcium, or zinc ions.[43] Nevertheless, except for the 3-fold channels, the 4-fold channels are also hydrophilic in phytoferritins.[11] For example, the 4-fold channel in plant ferritin is formed by histidine side chains (Figure 1B) composed of two layers.[11] Therefore, it is of special interest to elucidate the role of the 4-fold hydrophilic channels in iron oxidative deposition in phytoferritin, and the relationship with its analogues, 3-fold channels. The migration of Fe^{2+} through the protein shell to the ferroxidase center is one early event occurring prior to formation of the μ-peroxodiferric intermediate in ferritin.[16] The present studies demonstrate that similar to 3-fold channels, the 4-fold channels are also the main pathways for rapid iron entry into the protein.

To elucidate the function of the hydrophilic 4-fold channels in iron diffusion and oxidation in plant ferritin, three mutants including H193A/H197A (a 4-fold channel mutant), E165I/E176A/E171A (a 3-fold channel mutant), and E165I/E167A/E171A/H193A/H197A (a 3- and 4-fold channel mutant) were prepared (Figures 2 and 3) for the first time. Subsequently, the iron oxidation activities catalyzed by these three mutants were compared using rH-2 as control. It was found that, at low iron loadings (48 Fe^{2+}/shell), both the iron oxidation and oxygen consumption of H193A/H197A and E165I/E167A/E171A were blocked, indicating that the 4-fold channels are likewise important for iron diffusion and oxidation, similar to their 3-fold analogues. Thus, both 3- and 4-fold channels are involved in iron diffusion into the protein shell, followed by oxidation by oxygen. In agreement with this idea, E165I/E167A/E171A/H193A/H197A exhibits the lowest activity of iron oxidation among all three mutants (Figures 4A and 5A).

At medium iron loading (96 Fe^{2+}or 200 Fe^{2+}/shell), there is no marked difference in iron oxidation activity between the mutants. This is because most of the iron oxidation occurred on the outer surface of plant ferritin where the EP domains serve as the second ferroxidase center and are mainly responsible for iron oxidation (Figures 4B,C and 5B).[12] However, at high iron loading (500 Fe^{2+}/shell), both the EP and mineral core surface play an important role in iron oxidation. At this time, ferrous ions have to diffuse into protein cavity through the 3-fold or 4-fold channels, reaching the mineral core surface. It was observed that ferrous ion oxidation catalyzed by rH-2 was more rapid than that by its three variants (Figure 4D), again demonstrating that both the 3-fold channels and 4-fold channels are involved in the transfer of Fe^{2+} from its exterior surface to the cavity of the protein.

It has been recently reported that the binding and oxidation of iron occur at the EP located on the outer surface of the protein shell at iron loadings more than 48 Fe^{2+}/shell due to the low ferroxidase center regeneration activity of plant ferritin.[12,34] Resulting ferric ions binding on the protein outer surface induce aggregation of the protein into large assemblies. Subsequently, the bound ferric ions are gradually translocated to the protein cavity, during which the protein dissociates back into its monomeric state.[12] Such protein association only occurs upon addition of more than 48 Fe^{2+}/shell to apo plant ferritin. However, for the variants of rH-2, ferric-induced protein aggregation appeared even at low iron loading (Figure 6A), indicative of the difficulty of iron diffusion into the protein shell upon changing the polarity of the 3-fold and 4-fold channels from hydrophilic to hydrophobic. At medium iron loading (200 Fe^{2+}/shell), similar aggregations of rH-2 and its variants were observed by TEM.[14] At iron loading of 500 Fe^{2+}/shell, the mineral surface autoxidation reaction becomes increasingly important,[46] and the iron diffusion becomes the crucial process for iron oxidation, so protein association occurred with E165I/E167A/E171A/H193A/H197A to the greatest extent because all of the 3-fold and 4-fold hydrophilic channels became hydrophobic (Figure 6C), indicating that hydrophilic 3-fold and 4-fold channels are the main pathways for iron diffusion. This view was further supported by iron release results showing that ferric ions bound on the extension peptide of plant ferritin are rapidly released, and the iron release rate of E165I/E167A/E171A/H193A/H197A is the largest among all samples (Figure 7), due to the direct contact of reductants (ascorbic acid) and ferric ions without diffusion into protein cavity.

dx.doi.org/10.1021/bi500066m | *Biochemistry* 2014, 53, 2232−2241

The present results are in contrast with a recent report showing that the 3-fold channel is the only pathway for iron diffusion in animal ferritin.[16] Such a difference between animal and plant ferritins might stem from their different amino acids in the 4-fold channels; namely, the 4-fold channels in plant ferritin are hydrophilic, while they are hydrophobic in animal ferritin.[1−5] Interestingly, previous studies by Cho showed the translocation of iron through the 4-fold channels of ferritin from prokaryotes.[33] Thus, it appears that phytoferritin combines the characters of both the 3-fold channels from animal ferritin and the 4-fold channels from bacterial ferritin, employing both the 3- and 4-fold channels as iron diffusion pathways. From the viewpoint of evolution, prokaryotes, the iron diffusion pathway which is the 4-fold channels, are the history of life (plants, animals, etc.). In the development of life, plants appeared and the iron diffusion pathways of phytoferritin also evolved into 3-fold channels and 4-fold channels. Ferritin from animals evolved as well, and it only employed the 3-fold channels for iron diffusion. Therefore, both the 3- and 4-fold channels involved in iron diffusion in plant ferritin demonstrated in this work might be a result of evolution.[48]

In closing, the 4-fold channels of all known plant ferritin is hydrophilic, representing one major difference between animal and plant ferritn, but its function is unclear. The present work demonstrated that similar to the 3-fold channels, the 4-fold channels are likewise pathways for iron diffusion into the ferritin shell. This work defined the key features of the 4-fold channels in plant ferritin for oxidative deposition of iron in ferritin for the first time. These findings help in the understanding of the structure and function of ferritin.

■ ASSOCIATED CONTENT

Supporting Information

Association kinetics of ferritin detected by light scattering is shown in Figure S1. This material is available free of charge via the Internet at http://pubs.acs.org.

■ AUTHOR INFORMATION

Corresponding Authors

*(G.Z.) E-mail: gzhao@cau.edu.cn. Phone: +86-010-62738737. Fax: +86-010-62738737.

*(C.X.) E-mail: xcshan@163.com.

Funding

This work was supported by the National Natural Science Foundation of China (31271826) and the National Science and Technology Support Program (2011BAD23B04).

Notes

The authors declare no competing financial interest.

■ ACKNOWLEDGMENTS

Electron microscopy analysis was supported by the Beijing National Center for Electron Microscopy, Department of Materials Science and Engineering, Tsinghua University. We thank Dr. Taro Masuda for kindly providing the plasmid of rH-2.

■ ABBREVIATIONS

rH-2, recombinant soybean seed H-2 ferritin; rH-1, recombinant soybean seed H-1 ferritin; TEM, transmission electron microscopy; ROS, reactive oxygen species; TP, transit peptide; EP, extension peptide; SFER4, soybean seed H-4 subunit ferritin; CD, circular dichroism

■ REFERENCES

(1) Harrison, P. M., and Arosio, P. (1996) The ferritins: molecular properties, iron storage function and cellular regulation. *Biochim. Biophys. Acta 1275*, 161−203.

(2) Theil, E. C. (2003) Ferritin: at the crossroads of iron and oxygen metabolism. *J. Nutr. 133*, 1549S−1553S.

(3) Chasteen, N. D., and Harrison, P. M. (1999) Mineralization in ferritin: an efficient means of iron storage. *J. Struct. Biol. 126*, 182−194.

(4) Chasteen, N. D. (1998) Ferritin. Uptake, storage, and release of iron. *Met. Ions Biol. Syst. 35*, 479−514.

(5) Zhao, G. (2010) Phytoferritin and its implications for human health and nutrition. *Biochim. Biophys. Acta 1800*, 815−823.

(6) Crichton, R. R., Herbas, A., Chavez-Alba, O., and Roland, F. (1996) Identification of catalytic residues involved in iron uptake by L-chain ferritins. *J. Biol. Inorg. Chem. 1*, 567−574.

(7) Deng, J., Liao, X., Yang, H., Zhang, X., Hua, Z., Masuda, T., Goto, F., Yoshihara, T., and Zhao, G. (2010) Role of H-1 and H-2 subunits of soybean seed ferritin in oxidative deposition of iron in protein. *J. Biol. Chem. 285*, 32075−32086.

(8) Masuda, T., Goto, F., and Yoshihara, T. (2001) A novel plant ferritin subunit from soybean that is related to a mechanism in iron release. *J. Biol. Chem. 276*, 19575−19579.

(9) Ragland, M., Briat, J. F., Gagnon, J., Laulhere, J. P., Massenet, O., and Theil, E. C. (1990) Evidence for conservation of ferritin sequences among plants and animals and for a transit peptide in soybean. *J. Biol. Chem. 265*, 18339−18344.

(10) Lescure, A. M., Proudhon, D., Pesey, H., Ragland, M., Theil, E. C., and Briat, J. F. (1991) Ferritin gene transcription is regulated by iron in soybean cell cultures. *Proc. Natl. Acad. Sci. U.S.A. 88*, 8222−8226.

(11) Masuda, T., Goto, F., Yoshihara, T., and Mikami, B. (2010) Crystal structure of plant ferritin reveals a novel metal binding site that functions as a transit site for metal transferrin ferritin. *J. Biol. Chem. 285*, 4049−4059.

(12) Li, C., Fu, X., Qi, X., Hu, X., Chasteen, N. D., and Zhao, G. (2009) Protein association and dissociation regulated by ferric ion: a novel pathway for oxidative deposition of iron in pea seed ferritin. *J. Biol. Chem. 284*, 16743−16751.

(13) Fu, X., Deng, J., Yang, H., Masuda, T., Goto, F., Yoshihara, T., and Zhao, G. (2010) A novel EP- involved pathway for iron release from soyabean seed ferritin. *Biochem. J. 427*, 313−321.

(14) Yang, H., Fu, X., Li, M., Leng, X., Chen, B., and Zhao, G. (2010) Protein association and dissociation regulated by extension peptide: a mode for iron control by plant ferritin inseeds. *Plant Physiol. 154*, 1481−1491.

(15) Lee, J., Chasteen, N. D., Zhao, G., Papaefthymiou, G. C., and Gorun, S. M. (2002) Deuterium structural effects in inorganic and bioinorganic aggregates. *J. Am. Chem. Soc. 124*, 3042−3049.

(16) Bou-Abdallah, F., Zhao, G., Biasiotto, G., Poli, M., Arosio, P., and Chasteen, N. D. (2008) Facilitated diffusion of iron(II) and dioxygen substrates into human H-chain ferritin. A fluorescence and absorbance study employing the ferroxidase center substitution Y34W. *J. Am. Chem. Soc. 130*, 17801−17811.

(17) Bou-Abdallah, F., Arosio, P., Levi, S., Janus-Chandler, C., and Chasteen, N. D. (2003) Defining metal ion inhibitor interactions with recombinant human H-chain ferritins and site-directed variants. An isothermal titration calorimetry study. *J. Biol. Inorg. Chem. 8*, 489−497.

(18) Michaux, M. A., Dautant, A., Gallois, B., Granier, T., d'Estaintot, B. L., and Precigoux, G. (1996) Structural investigation of the complexation properties between horse spleen apoferritin and metalloporphyrins. *Proteins 24*, 314−321.

(19) Barnés, C. M., Theil, E. C., and Raymond, K. N. (2002) Iron uptake in ferritin is blocked by binding of $[Cr(TREN)(H_2O)(OH)]^{2+}$, a slow dissociating model for $[Fe(H_2O)_6]^{2+}$. *Proc. Natl. Acad. Sci. U.S.A. 99*, 5195−5200.

(20) Li, M., Yun, S., Yang, X., and Zhao, G. (2013) Stability and iron oxidation properties of a novel homopolymeric plant ferritin from adzuki bean seeds: A comparative analysis with recombinant soybean seed H-1 chain ferritin. *Biochim. Biophys. Acta 1830*, 2946−2953.

(21) Masuda, T., Goto, F., Yoshihara, T., Ezure, T., Takashi, S., Kobayashi, S., Shikata, M., and Utsumi, S. (2007) Construction of homo- and heteropolymers of plant ferritin subunits using an in vitro protein expression system. *Protein Expression Purif. 56*, 237−246.
(22) Laemmli, U. K. (1970) Cleavage of structural proteins during the assembly of the head of bacteriophage T4. *Nature 227*, 680−685.
(23) Yang, X., Chen-Barrett, Y., Arosio, P., and Chasteen, N. D. (1998) Reaction paths of iron oxidation and hydrolysis in horse spleen and recombinant human ferritins. *Biochemistry 37*, 9743−9750.
(24) Meldrum, F. C., Wade, W. J., Nimmo, D. L., Heywood, B. R., and Mann, S. (1991) Synthesis of inorganic nano phase materials in supramolecular protein cages. *Nature 349*, 684−687.
(25) Hynes, M. J., and Coinceanainn, M. O. (2002) Investigation of the release of iron from ferritin by naturally occurring antioxidants. *J. Inorg. Biochem. 90*, 18−21.
(26) Zamorano, L. S., Pina, D. G., Gavilanes, F., Roig, M. G., Sakharov, I. Y., Jadan, A. P., Van Huystee, R. B., Villar, E., and Shnyrov, V. L. (2004) Two-state irreversible thermal denaturation of anionic peanut (Arachis hypogaea L.) peroxidase. *Thermochim. Acta 417*, 67−73.
(27) Deng, J., Li, M., Zhang, T., Chen, B., Leng, X., and Zhao, G. (2011) Binding of proanthocyanidins to soybean (Glycine max) seed ferritin inhibiting protein degradation by protease in vitro. *Food Res. Int. 44*, 33−38.
(28) Amisha Kamal, A. J., and Behere, D. V. (2001) Steady-state and picosecond timeresolved fluorescence studies on native and apo seed coat soybean peroxidase. *Biochem. Biophus. Res. Comm. 289*, 427−433.
(29) Yang, X., Le Brun, N. E., Thomson, A. J., Moore, G. R., and Chasteen, N. D. (2000) The iron oxidation and hydrolysis chemistry of *Escherichia coli* bacterioferritin. *Biochemistry 39*, 4915−4923.
(30) Bou-Abdallah, F., Lewin, A. C., Le Brun, N. E., Moore, G. R., and Chasteen, N. D. (2002) Iron detoxification properties of *Escherichia coli* bacterioferritin. attenuation of oxyradical chemistry. *J. Biol. Chem. 277*, 37064−37069.
(31) Bou-Abdallah, F., Zhao, G., Mayne, H. R., Arosio, P., and Chasteen, N. D. (2005) Origin of the unusual kinetics of iron deposition in human H-chain ferritin. *J. Am. Chem. Soc. 127*, 3885−3893.
(32) Crichton, R. R., and Roman, F. (1978) A novel mechanism for ferritin iron oxidation and deposition. *J. Mol. Catal. 4*, 75−82.
(33) Cho, K. J., Shin, H. J., Lee, J. H., Kim, K. J., Park, S. S., Lee, Y., Lee, C., Park, S. S., and Kim, K. H. (2009) The crystal structure of ferritin from *Helicobacter pylori* reveals unusual conformational changes for iron uptake. *J. Mol. Biol. 390*, 83−98.
(34) Li, C., Hu, X., and Zhao, G. (2009) Two different H-type subunits from pea seed (*Pisum sativum*) ferritin that are responsible for fast Fe(II) oxidation. *Biochimie 91*, 230−239.
(35) Turano, P., Lalli, D., Felli, I. C., Theil, E. C., and Bertini, I. (2010) NMR reveals pathway for ferric mineral precursors to the central cavity of ferritin. *Proc. Natl. Acad. Sci. U.S.A. 107*, 545−550.
(36) Wade, V. J., Arosio, P., Treffry, A., Harrison, P. M., and Mann, S. (1991) Influence of site-directed modifications on the formation of iron cores in ferritin. *J. Mol. Biol. 221*, 1443−1452.
(37) Macara, I. G., Hoy, T. G., and Harrison, P. M. (1972) The formation of ferritin from apoferritin. Kinetics and mechanism of iron uptake. *Biochem. J. 126*, 151−162.
(38) Galvez, N., Fernandez, B., Sanchez, P., Cuesta, R., Ceolin, M., Clemente-Leon, M., Trasobares, S., Lopez-Haro, M., Calvino, J. J., Stephan, O., and Dominguez-Vera, J. M. (2008) Comparative structural and chemical studies of ferritin cores with gradual removal of their iron contents. *J. Am. Chem. Soc. 130*, 8062−8068.
(39) Zhao, G., Bou-Abdallah, F., Arosio, P., Levi, S., Janus-Chandler, C., and Chasteen, N. D. (2003) Multiple pathways for mineral core formation in mammalian apoferritin. The role of hydrogen peroxide. *Biochemistry 42*, 3142−3150.
(40) Lv, C., Bai, Y., Yang, S., Zhao, G., and Chen, B. (2013) NADH induces iron release from pea seed ferritin: A model for interaction between coenzyme and protein components in foodstuffs. *Food Chem. 141*, 3851−3858.
(41) Arosio, P., Ingrassia, R., and Cavadini, P. (2009) Ferritins: a family of molecules for iron storage, antioxidation and more. *Biochim. Biophys. Acta 1790*, 589−599.
(42) Lawson, D. M., Artymiuk, P. J., Yewdall, S. J., Smith, J. M., Livingstone, J. C., Treffry, A., Luzzago, A., Levi, S., Arosio, P., Cesareni, G., Thomas, C. D., Shaw, W. V., and Harrison, P. M. (1991) Solving the structure of human H-ferritin by genetically engineering intermolecular crystal contacts. *Nature 349*, 541−544.
(43) Hempstead, P. D., Yewdall, S. J., Fernie, A. R., Lawson, D. M., Artymiuk, P. J., Rice, D. W., Ford, G. C., and Harrison, P. M. (1997) Comparison of the three-dimensional structures of recombinant human H and horse L ferritins at high resolution. *J. Mol. Biol. 268*, 424−448.
(44) Stillman, T. J., Hempstead, P. D., Artymiuk, P. J., Andrews, S. C., Hudson, A. J., Treffry, A., Guest, J. R., and Harrison, P. M. (2001) The high-resolution X-ray crystallographic structure of the ferritin (EcFtnA) of Escherichia coli; comparison with human H ferritin (HuHF) and the structures of the Fe(3+) and Zn(2+) derivatives. *J. Mol. Biol. 307*, 587−603.
(45) Chichton, R. R., and Declercq, J. P. (2010) X-ray structure of ferritins and related proteins. *Biochim. Biophys. Acta 1800*, 706−718.
(46) Le Brun, N. E., Crow, A., Murphy, M. E. P., Mauk, A. G., and Moore, G. R. (2010) Iron core mineralization in prokaryotic ferritins. *Biochim. Biophys. Acta 1800*, 732−744.
(47) Treffry, A., Zhao, Z., Quail, M. A., Guest, J. R., and Harrison, P. M. (1998) How the presence of three iron binding sites affects the iron storage function of the ferritin (EcFtnA) of *Escherichia coli*. *FEBS Lett. 432*, 213−218.
(48) Waters, E. R. (2003) Molecular adaptation and the origin of land plants. *Mol. Phylogenet. Evol. 29*, 456−463.